Immobilization of a Full Photosystem in the Large-Pore MIL-101 Metal-Organic Framework for CO2 reduction

X. Wang, F. Wisser, J. Canivet, M. Fontecave, C. Mellot-Draznieks

Immobilization of a full photosystem in the large pore MIL-101 Metal-organic Framework for CO_2 reduction

Xia Wang,[a] Florian M. Wisser,[b] Jérôme Canivet,[b] Marc Fontecave,*[a] Caroline Mellot-Draznieks*[a]

Abstract: A molecular catalyst $[Cp^*Rh(4,4'\text{-bpydc})]^{2+}$ and a molecular photosensitizer $[Ru(bpy)_2(4,4'\text{-bpydc})]^{2+}$ (bpydc = bipyridinedicarboxylic acid) were successfully co-immobilized into the highly porous metal-organic framework MIL-101-NH_2 upon easy post-synthetic impregnation. The Rh-Ru@MIL-101-NH_2 composite allows the reduction of CO_2 under visible light, while exhibiting remarkable selectivity with the exclusive production of formate. This Rh-Ru@MIL-101-NH_2 solid represents the first example of MOFs functionalized with both a catalyst and a photosensitizer in a non-covalent fashion. Thanks to the co-confinement of the catalyst and photosensitizer into the cavity's nanospace, the MOF pores are used as nanoreactors and allow performing molecular catalysis in a heterogeneous manner.

Introduction

The conversion of the greenhouse gas CO_2 into valuable fuels and chemicals such as CO, formic acid, hydrocarbons and alcohols *via* photocatalysis is the subject of increasingly intense research efforts, driven in particular by the incentive of using solar energy as an inexpensive and renewable source of energy. While photosystems for CO_2 reduction based on molecular catalysts and molecular photosensitizers assisted by a sacrificial electron donor have been extensively studied, only a few have been heterogenized, as a necessary step for practical applications.[1] Recently, metal-organic frameworks (MOFs) - a class of porous crystalline structures composed of organic and inorganic building blocks- have emerged as potentially interesting platforms for designing heterogeneous porous photocatalysts, [2] thanks to their versatility whereby mixed-linker synthesis strategies or post-synthetic modifications allow their functionalization. [3] In particular, the incorporation of both metal-centered molecular catalysts and light-harvesting antennas into their framework or pores has opened the way to the co-engineering of their catalytic and optical properties.[4] There are thus abundant reports of functionalized MOF-based solids that possess photocatalytic activities in order to catalyze organic transformations,[5] water oxidation,[6] proton reduction,[7] or CO_2 reduction.[8]

A sub-class of MOFs made of metal-free organic linkers exhibit photocatalytic activities for CO_2 reduction, whereby their metal-oxide nodes act as catalysts (cat) while their linkers act as photosensitizers (PS). [9] Topical examples include the aminated terephtalate-based MIL-125-NH_2[9a-b] and UiO-66-NH_2[9c-e] or porphyrin-based MOFs.[9g] Importantly, these MOFs all exhibit adequate electronic band structures for allowing LMCT (ligand-to-metal-charge-tranfer) within their hybrid scaffold.[10] Besides these MOFs, various strategies have been developed to functionalize MOFs' scaffold with organometallic species which may serve as antenna and/or catalysts for the reduction of CO_2. For example, bipyridine (bpy) containing linkers with dicarboxylic acid functionalities may be used to prepare metallated linkers, either by one-pot-synthesis or by post-synthetic exchange. Following this strategy initiated by Lin *et al.* in 2011,[4a] a sub-class of functionalized MOFs has emerged, for example derived from the robust Zr(IV)-based UiO-67[11] or Al(III)-based DUT-5/MOF-253[12] to name but a few, possessing open chelating groups such as bipyridines or catechols complexed with transition metals such as Re-,[4a,13] Ru-[14], Rh-[15] or Mn.[16] Many of those heterogeneous catalysts require the use of an additional PS in solution such as $[Ru(bpy)_3]^{2+}$. Still, in such cases where MOF-supported catalysts are used with molecular homogeneous PS, a diffusion limitation may occur whereby the access to the active site for the PS may be restricted, thus lowering the catalytic activity. Alternatively fully heterogeneous systems allowing the covalent embedding of both PS and cat into the MOF as a part of its scaffold have been recently reported in bypiridine-based MOFs.[17] In this case, the fixed positions of site-isolated PS and cat within the rigid framework structure impose the electron transfer from PS to cat to proceed through space or along the framework structure. Moreover, covalent attachment of species with catalytic or photosensitizing functions within a MOF, by one-pot synthesis or post-synthesis, is not a trivial issue.

Another more simple strategy consists in encapsulating or immobilizing catalytic active species, *i.e.* through non-covalent interactions, into the pores of the MOF through one-pot-synthesis or a post-synthetic impregnation.[18] These catalytic systems can be used in photocatalysis in the presence of a photosensitizer either in solution or covalently immobilized within the MOF scaffold. Such immobilization strategies have been valuably developed for designing MOF-based photocatalytic systems for water oxidation and proton reduction.[19] More recently, we have reported the photosensitization of an immobilized cobalt-polyoxometallate into the pores of the porphyrin-based MOF-545 for the oxidation of water.[20] Notably, no photosystem of this type has been reported for the reduction of CO_2 so far.

Here, we explore for the first time a "tea bag" strategy whereby both the catalyst and the photosentisizer are irreversibly co-immobilized upon easy post-synthetic impregnation in the porous MOF host, with a {PS, cat} combination selected for CO_2 photoreduction. Using the MOF cavity as a nanoreactor allows confining intimately the molecular active species into the cavity's nanospace to perform molecular catalysis in a heterogeneous manner. By investigating the adsorption of both cat and PS species, we prepared a new hybrid photosystem which is evaluated for the catalyzed CO_2-to-formate photoreaction under visible light irradiation.

Results and discussion

[a] Dr. X. Wang, Prof. M. Fontecave, Dr. C. Mellot-Draznieks
Laboratoire de Chimie des Processus Biologiques (LCPB), Collège de France, PSL Research University, CNRS, Sorbonne Universités, 11 Marcelin Berthelot, 75231 Paris Cedex 05, France
Fax: +33 1 44271356 ; Tel: +33 1 44271213
E-mail: caroline.mellot-draznieks@college-de-france.fr
[b] Dr. F. M. Wisser, Dr. J. Canivet
Univ. Lyon, Université Claude Bernard Lyon 1, CNRS, IRCELYON - UMR 5256, 2 Avenue Albert Einstein, 69626 Villeurbanne Cedex, France
Supporting information for this article is given via a link at the end of the document.

We have selected the MIL-101-NH_2(Al) metal-organic framework as an efficient inert platform (*i.e.* with no photocatalytic activity for CO_2 reduction) for the co-immobilization of cat and PS thanks to its large pore diameter which is able to accommodate large size molecules (**Figure 1**). MIL-101-NH_2(Al) is a pale yellow solid, while its Cr- and Fe- counterparts are dark green and dark brown, respectively. We infer that the much lower light absorption of MIL-101-NH_2(Al) will allow photons to reach more efficiently PS molecules immobilized in MIL-101-NH_2(Al) while MIL-101-NH_2 (Cr/Fe) would absorb light and thus competing with the molecular photosensitizer.

MIL-101-NH_2(Al) is isostructural to the three-dimensional (Cr)MIL-101 crystal structure and is formed of octahedral trimeric Al(III) clusters linked by 2-aminoterephthalate ligands.[21] Two types of mesoporous quasi-spherical cages exist in MIL-101: (i) cages of 20 supertetrahedra with a free diameter of 29 Å accessible through a pentagonal window of 12 Å aperture (green cages in **Figure 1**); (ii) larger cages delimited by 28 supertetrahedra and a free diameter of 34 Å accessible through additional hexagonal windows with a 14.7 Å * 16 Å aperture (red cage in **Figure 1**). Besides its mesoporosity, the aminated form of MIL-101, *i.e.* MIL-101-NH_2, was chosen as an interesting chemical derivative in order to favor host-guest interactions such as hydrogen bonds between the {PS, cat} photosystem and the MOF host.

The MIL-101-NH_2(Al) material was synthesized according to reported procedures.[22] In a preliminary step, we studied the immobilization of the single PS or Cat species in (Al)MIL-101- NH_2 in order to determine the conditions for their irreversible adsorption. MIL-101-NH_2(Al) (5 mg) was dispersed in a 4 mL solution of acetonitrile (MeCN) prepared at a pre-defined concentration of PS or cat. The depletion of PS or cat complex-es from the solution due to their adsorption into the MOF was monitored at hourly time intervals by UV-visible spectroscopy of the supernatant solution (see SI for details). Indeed, the adsorption of the soluble PS or cat compound by the MOF results in a decrease of characteristic absorption bands intensities. Similarly, the release of PS (or cat) from the PS@MOF (or cat@MOF) solid after encapsulation can be studied by exposing the impregnated material repeatedly to fresh MeCN and by monitoring the compound released in solution by UV-Vis spectroscopy.

A series of candidate photosensitizers were evaluated for immobilization in MIL-101-NH_2 (**Figure S1**). Besides $[Ru(bpy)_3]Cl_2$, one of the most commonly used PS in photocatalysis, we also investigated a couple of carboxylated derivatives containing one 2,2'-bipyridine-4,4'-dicarboxylic acid (4,4'-bpydc) or 2,2'-bipyridine-5,5'-dicarboxylic acid (5,5'-bpydc) ligand, namely $[Ru(bpy)_2(4,4'\text{-bpydc})](PF_6)_2$ and $Ru(bpy)_2(5,5'\text{-bpydc})](PF_6)_2$. Our choice here was guided by the fact that carboxylic acid groups may favor additional hydrogen bond type host-guest interactions between PS and MOF's chemical groups, such as amino groups, water molecules or -OH groups coordinated to the inorganic sub-network of MIL-101-NH_2, as further confirmed by our DFT calculations (*vide infra*).

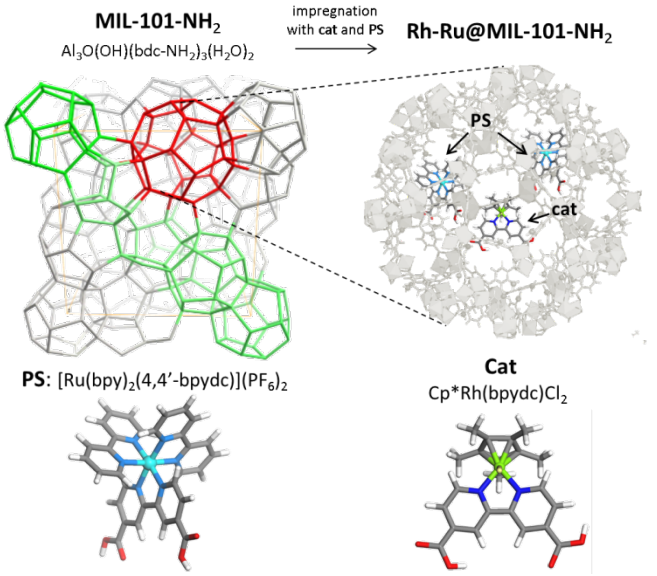

Figure 1. Schematic representation of co-immobilized photosystem in in MIL-101-NH_2 showing the host topology with its small (green) and large (red) cages and enlarged large cage of Rh-Ru@MIL-101-NH_2 (upper part). Lower part showing the enlarged structures of photosensitizer (PS) $Ru(bpy)_2(4,4'\text{-bpydc})](PF_6)_2$, and catalyst (cat) $Cp^*Rh(4,4'\text{-bpydc})Cl_2$ (O: red, N: blue, Ru: cyan, Rh: green, C: grey, H: white). Counter anions are omitted for clarity.

Performing the impregnation of 5 mg of MIL-101-NH_2 with 0.1 mM solutions of $[Ru(bpy)_3]Cl_2$, $[Ru(bpy)_2(4,4'\text{-bpydc})](PF_6)_2$ or $Ru(bpy)_2(5,5'\text{-bpydc})](PF_6)_2$ in 4 ml MeCN, we compared the time evolution of UV-Vis absorption spectra of the three supernatant solutions (**Figures 2a** and **S2**). The gradual uptake of each Ru-based PS into MIL-101-NH_2(Al) was systematically observed as probed by the time-dependent decrease of the strong characteristic bands of the PS in the supernatant solution, typically in the 420-470 nm region (assigned to Metal Ligand Charge Transfer, MLCT). Notably, the time evolution of the UV-Vis spectra of the carboxylated Ru-complexes exhibited distinctive features when compared to those of the non-carboxylated one. First uptake into MIL-101-NH_2(Al) is much faster: uptake of ~40% (0.16 μmol) over 1h is observed for both carboxylated photosensitizers (**Figures S2b-c**) to be compared with a slower uptake to reach a maximum of ~30% (0.12 μmol) after 3 h reaction in the case of the non-carboxylated complex, $[Ru(bpy)_3]Cl_2$ (**Figure S2a**). Second, we did not observe any release of the carboxylated PS from the PS@MOF solid after more than 20 h exposure to a fresh MeCN solution, in clear contrast with $[Ru(bpy)_3]Cl_2$ which was slowly released in solution under identical conditions (**Figure S2a, inset**). Using Beer-Lambert law we estimated from the intensities of the absorption band at 430 nm that 0.2 μmol of $[Ru(bpy)_2(4,4'\text{-bpydc})](PF_6)_2$ and $[Ru(bpy)_2(5,5'\text{-bpydc})](PF_6)_2$ present in solution were irreversibly adsorbed into 5 mg MIL-101-NH_2(Al) in 24 h. Also, the similar uptake observed for the 4,4'-bpydc and 5,5'-bpydc derivatives suggest that the position of the carboxylic acid groups in the PS complex did not affect its adsorption equilibrium in (Al)MIL-101-NH_2.

Considering candidate catalysts (cat) for CO_2 reduction, we selected various Cp*Rh-based (Cp* = pentamethylcyclo-

pentadienyl) complexes for impregnation experiments in MIL-101-NH_2. Cp*Rh based complexes have been reported to perform the catalytic reduction of NAD^+ cofactor[23] and Cp*Rh(bpy)Cl_2 is known to catalyze the electrochemical reduction of CO_2 into formate, however together with a significant production of H_2.[24] We recently reported the first photosensitization of the Cp*Rh(bpy)Cl_2 complex when heterogenized into the UiO-67 metal-organic framework as a constitutive linker, *i.e.* Cp*Rh@UiO-67,[15] or into bipyridine-containing microporous polymers,[25] allowing the reduction of CO_2 into formate, with H_2 formation in parallel, under photocatalytic conditions. This Rh-based catalytic complex thus represents an ideal candidate to investigate a full {cat, PS} photosystem non-covalently immobilized within a porous host for CO_2 reduction.

The impregnation of 5 mg MIL-101-NH_2(Al) with the $[Cp^*RhCl_2]_2$ synthetic precursor and non-carboxylated [Cp*Rh(bpy)Cl]Cl catalyst, 0.1 mM MeCN solution, was considered. In addition, having in mind the beneficial impact of carboxylic groups found above for favoring the immobilization of the PS, two carboxylated catalysts, namely [Cp*Rh(4,4'-bpydc)Cl]Cl and [Cp*Rh(5,5'-bpydc)Cl]Cl, were also studied. The time evolution of UV-Vis spectra using the non-carboxylated complexes, $(Cp^*RhCl_2)_2$ and [Cp*Rh(bpy)Cl]Cl, revealed relatively poor impregnation rates into MIL-101-NH_2 (**Figures S4-a-b**). By contrast, both carboxylated Rh-catalysts, [Cp*Rh(4,4'-bpydc)Cl]Cl and [Cp*Rh(5,5'-bpydc)Cl]Cl, were efficiently adsorbed into MIL-101-NH_2 with 70-80% uptake over 1h *i.e.* 0.32 μmol per 5mg of MOF. Their irreversible immobilization is shown by a total lack of leaching (**Figures 2b and S4d,** insets) confirmed the beneficial role of -COOH groups.

For preparing the full photosystem for CO_2 reduction, we selected the carboxylated versions of cat and PS, *i.e.* [Cp*Rh(4,4'-bpydc)Cl]Cl and [Ru(bpy)$_2$(4,4'-bpydc)]$(PF_6)_2$, respectively for their co-immobilization into (Al)MIL-101-NH_2, named Rh-Ru@MIL-101-NH_2. The 4,4'-bpydc based cat complex is of particular interest considering that –COOH groups in the 4,4'-position should result in a higher electron density on the catalytic center and hence a higher catalytic activity. [25,26] The cat and PS co-impregnation in 75 mg MIL-101-NH_2(Al) was performed as described above by using a mixture of [Cp*Rh(4,4'-bpydc)Cl]Cl and [Ru(bpy)$_2$(4,4'-bpydc)]$(PF_6)_2$ in MeCN and monitored by UV-Vis spectroscopy of the supernatant solution (**Figure S5**). We observed that a cat:PS ratio of 1:5 (3.3 μmol cat and 16.5 μmol PS) in MeCN solution allowed the adsorption in a 1:2 ratio of immobilized species in Rh-Ru@MIL-101-NH_2 as confirmed by ICP-OES and liquid state ^{1}H NMR spectroscopy of the digested MOF (**see SI, Figure S6)**.

ICP-OES elemental analysis of Rh-Ru@MIL-101-NH_2 (Chemical Anal. found: Al 8.71±0.57%, Ru 0.61±0.03%, Rh 0.32±0.02%. see **Table S1**) allows proposing the following chemical formula $[Al_3O(OH)(bdc\text{-}NH_2)_3(H_2O)_2]_{24}$, [Cp*Rh(4,4'-bpydc)Cl]Cl, [Ru(bpy)$_2$(4,4'-bpydc)]$(PF_6)_2]_2$.*n* H_2O. (*n* is estimated ~200 from TGA, **Figure S7**) and confirms the amount of immobilized complexes established by UV-Vis spectroscopy, *i.e.* one Rh-catalytic complex and 2 PS molecules per large cage on average. We considered this average of 1 cat for 2 PS per cage as appropriate to allow the isolation of Rh-catalytic sites while avoiding crowding the cages with PS molecules.

The Rh-Ru@MIL-101-NH_2 solid was further characterized with various physical techniques. The comparison of the powder X-ray diffraction patterns of the pristine MIL-101-NH_2(Al) and of Rh-Ru@MIL-101-NH_2 confirms that the crystallinity of the MOF host is maintained upon the co-immobilization of both Rh- and

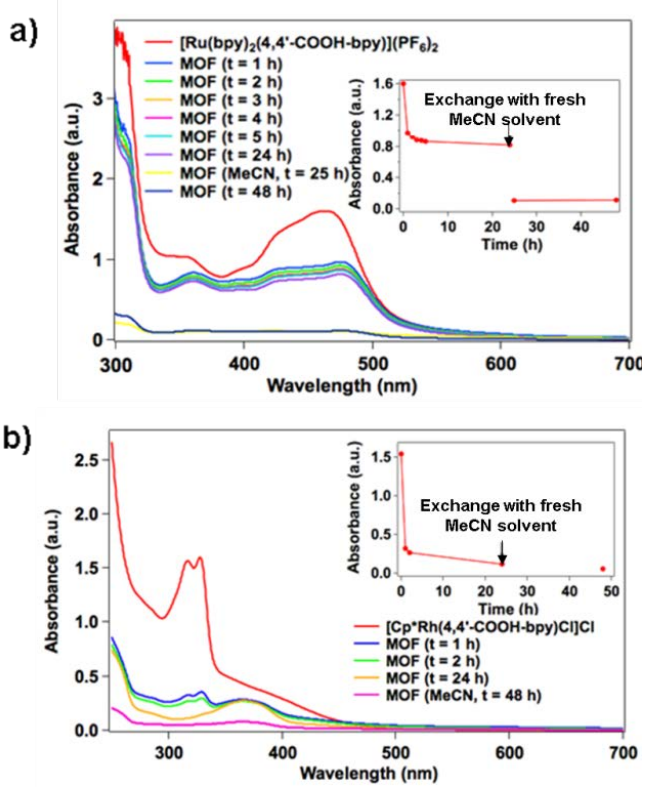

Figure 2. Time evolution of the UV-Vis absorption spectra of (a) 0.1 mM [Ru(bpy)$_2$(4,4'-bpydc)]$(PF_6)_2$ and (b) 0.1 mM [Cp*Rh(4,4'-bpydc)Cl]Cl in MeCN in the absence (red) and presence of 5 mg MIL-101-NH_2 (blue to pink). Insets: time evolution of the absorption band at 319 nm (cat) and at 465 nm (PS). After 24 h, the supernatant is removed and fresh MeCN is added (see arrow); no release of Ru- (a) and Rh-complexes (b) was detected.

Ru-complexes (**Figure 3a**). Brunauer–Emmett–Teller (BET) surface areas calculated from N_2 adsorption isotherms shows the expected correlation between decreased surface areas and {cat, PS} immobilization into the large pores, from 2100 m^2g^{-1} for the pristine MIL-101-NH_2(Al) to 1570 m^2g^{-1} for the Rh-Ru@MIL-101-NH_2 material (**Figure 3b**). Also, the solid state UV-Vis spectrum of Rh-Ru@MIL-101-NH_2 (**Figure S8**) merges the characteristic intense bands of the MIL-101-NH_2(Al) solid in the 350-400 nm range (π → π* transition), and those of [Ru(bpy)$_2$(4,4'-bpydc)]$(PF_6)_2$ apparent in the 450-650 nm range (MLCT), thus corroborating the effective immobilization of the PS complex into the MOF. The weaker absorption bands of the Rh-catalyst fall within the 300-400 nm region of the intense band of the MIL-101-NH_2(Al) framework and cannot be assigned.

The XPS spectra confirm the chemical composition of the Rh-Ru@Mil-101-NH_2 as well as the oxidation state of the photosensitizer and the catalyst (**Figures S10-S12**). Overall, all these data confirmed the co-immobilization of both Rh and Ru-complexes within MIL-101-NH_2's pores.

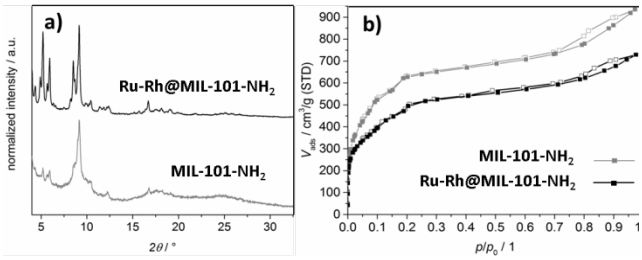

Figure 3. (a) Powder X-ray diffraction patterns ($Cu_{K\alpha}$) and (b) BET N_2 adsorption isotherms (77 K) of the pristine MIL-101-NH_2(Al) (grey) and Ru-Rh@MIL-101-NH_2 (black) solids.

To probe the {MOF, catalyst} interface and the most likely positions of the Rh-complex within MIL-101-NH_2(Al) pores, we applied a combination of Monte Carlo simulated annealing (SA) and Density Functional Theory (DFT) calculations. Using a periodic model of MIL-101-NH_2(Al) crystal structure, SA calculations allowed identifying a series of possible favorable positions of the Rh-catalyst. Further geometry optimizations at the DFT-dispersion corrected (DFT-D3) level were performed on clusters derived from SA calculations (See text in SI for details) to scrutinize the {MOF, catalyst} interface. Two favored conformations were considered at the DFT level, the most favorable one being illustrated in **Figure 4**. In this position, the Rh-complex establishes interactions within the hybrid framework through two hydrogen-bonds at 1.9 Å each. These emanate from a single carboxylic group of the Rh-complex interacting with a terminal water molecule of an inorganic sub-unit and with one amino group of a neighboring linker. An additional π–π interaction at 4.2 Å provides further stabilization between the Cp* moiety of the Rh-complex and the phenyl ring of an adjacent aminated linker. In a second less favorable position (**Figure S13**), the anchorage of the Rh-complex at the MOF surface is weaker, whereby only a single H-bond is established between a -COOH group and a neighboring water molecule. Consistently, the DFT calculations indicate that host-guest interactions in the first position are stronger than in the latter by more than 34 kJ. mol^{-1}.

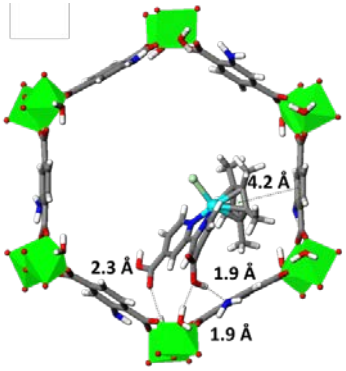

Figure 4. Rh-complex in MIL-101-NH_2. The cat@MOF system was geometry optimized at the DFT-D3 level. Stabilization is provided by H-bonds between –COOH of the Rh-complex and $H_2O_{(MOF)}$ and by π–π interaction between the Cp moiety of the Rh-complex and one ATA linker. (O: red, N: blue, Rh: turquoise; C: grey, H: white; AlO_6 octahedra: green).

We first studied the stability of the Rh-Ru@MIL-101-NH_2 composite in MeCN-triethanolamine (MeCN:TEOA) solutions, TEOA being required both as a sacrificial electron donor and as a proton source in photocatalytic essays for CO_2 reduction. These experiments were performed dispersing 5 mg of Rh-Ru@MIL-101-NH_2 in 4 mL of three MeCN:TEOA solutions differing by their volumetric ratios (5:1, 10:1 and 20:1). The liquid UV-Vis spectra of the supernatant solutions were recorded after 24 h in each case (**Figure S14**). It is apparent that larger concentrations in TEOA resulted in a stronger band centered at 345 nm (assigned to aminated terephtalate linker) and in the 400-500 nm region (assigned to the Ru-complex) implying a more pronounced dissolution of the MOF and in consequence the enhanced release of immobilized complexes. Trying to decrease the magnitude of this phenomenon, we find that a MeCN:TEOA ratio of 20:1 (*V*:*V*) allows preserving the integrity of the Ru-Rh@MIL-101-NH_2 composite while minimizing the release of Ru-complex down to ~1%. Under these conditions, the crystallinity of the Ru-Rh@MIL-101-NH_2 material is well preserved as shown by the similarity of the PXRD patterns of Rh-Ru@MIL-101-NH_2 exposed to the MeCN:TEOA solution (20:1) and that of the pristine MIL-101-NH_2 (**Figure S15**), making MeCN:TEOA (20:1) solution appropriate for further photocatalytic investigations.

The photocatalytic assays for CO_2 reduction were performed under UV light irradiation with a 425 nm cut-off filter in a 1 cm quartz cuvette maintained at 20°C using CO_2-saturated MeCN:TEOA (20:1, *V*:*V*) as the solvent. The amount of assayed Ru-Rh@MIL-101-NH_2 (2.5 mg) corresponds to 0.1 μmol cat and 0.2 μmol PS. Remarkably, formate is the only product observed upon exposure to light, as no traces of CO or H_2 could be detected. As shown in **Figure 5**, formate immediately formed upon exposure to light and increased quasi-linearly with time over the first 10 h, with slower rates over the next 10 h. Control experiments with i) the pristine MIL-101-NH_2(Al) , *i.e.* with no cat and no PS (**Table 1**, entry 2), ii) Rh@MIL-101-NH_2 alone (**Table 1**, entry 3) and iii) Ru@MIL-101-NH_2 alone (**Table 1**, entry 4) resulted into basal production of formate. Another control (Table 1, entry 5) was performed in order to compare the performance of the fully heterogeneous Rh-Ru@MIL-101-NH_2 photosystem to that of the Rh@MIL-101-NH_2 catalyst in the presence of $Ru(bpy)_3]Cl_2$ in solution, *i.e.* with the PS component not immobilized into the MOF (hence the use of the non-carboxylated Ru-complex). The photocatalytic activity of this system accounted for only ~50% of that of Rh-Ru@MIL-101-NH_2. This control illustrates the benefit of co-immobilizing the PS and the cat molecular complexes into the host (Al)MIL-101-NH_2, achieved here using a carboxylated versions of both Ru- and Rh- complexes as a likely result of the confinement of both the PS and cat within the MOF's pores.

The most remarkable property of the Rh-Ru@MIL-101-NH_2 photosystem is its overall selectivity for formate production (**Table 1**, entry 1). This is in marked contrast with the corresponding fully homogenous system which led to H_2 as the major product (Table 1, entry 6). This latter feature points to a role of the MOF host in altering the selectivity of the reduction reaction, via inhibition of proton reduction, when compared to

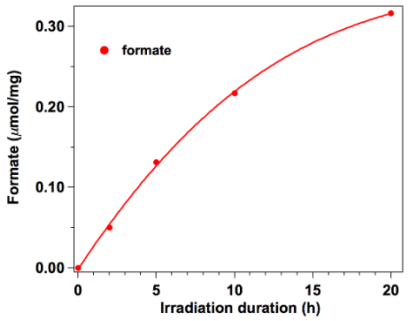

Figure 5. Formate production catalyzed by 2.5 mg Rh-Ru@MIL-101-NH_2 containing 0.1 μmol of [Cp*Rh(4,4'-bpydc)Cl]Cl and 0.2 μmol of [Ru(bpy)$_2$(4,4'-bpydc)](PF6)$_2$ in 1 mL of CO_2-saturated MeCN:TEOA (20:1) solvent mixture upon irradiation with a 300 W Xe arc lamp equipped with a 415 nm filter. 2.5 mg of hybrid Rh-Ru@MIL-101-NH_2 were used for each photocatalytic assays.

Table 1. Formate production for Rh-Ru@MIL-101-NH_2-catalyzed CO_2 reduction and controls. All experiments were carried out with the same batch of MIL-101-NH_2.

Entry	Photosystem	μmol	
		formate	H_2
1	Ru-Rh@MIL-101-NH_2 [a]	0.33	0
2	MIL-101-NH_2 [b]	0.02	0
3	Rh@MIL-101-NH_2 [c]	0.02	0
4	Ru@MIL-101-NH_2 [d]	0.02	0
5	Rh@MIL-101+[Ru(bpy)$_3$]Cl$_2$ [e]	0.16	0
6	Rh + Ru in solution [f]	0.04	1.9

The number of moles of product are given after 5 h for 1 mL of CO_2-saturated MeCN-TEOA (20:1) solvent using a 300 W Xe arc lamp with a 415 nm filter. [a]assay for 2.5 mg Rh-Ru@MIL-101 (containing 0.1 μmol cat and 0.2 μmol PS) performed in the kinetic study. [b]assay for 2.5 mg of the pristine MOF. [c]assay for 0.1 μmol of [Cp*Rh(4,4'-bpydc)Cl]Cl encapsulated in MIL-101-NH_2. [d]assay for 0.2 μmol of [Ru(bpy)$_2$(4,4'-bpydc)](PF$_6$)$_2$ encapsulated in MIL-101-NH_2, in the absence of Rh complex. [e] assay for 0.1 μmol of [Cp*Rh(4,4'-bpydc)Cl]Cl encapsulated in MIL-101-NH_2 with 0.2 μmol of [Ru(bpy)$_3$]Cl$_2$ in solution. [f] Fully homogeneous system containing 0.1 μmol of [Cp*Rh(4,4'-bpydc)Cl]Cl and 0.2 μmol of [Ru(bpy)$_2$(4,4'-bpydc)](PF$_6$)$_2$.

the homogeneous conditions (entry 6). The absence of H_2 in the Rh-Ru@MIL-101-NH_2 dependent system provides further indirect evidence that no significant co-leaching of cat and PS out from the Rh-Ru@MIL-101-NH_2 material to the solution occurs during photocatalysis. Along this line, the residual solution after photocatalysis was characterized by UV-Vis spectroscopy showing that no free cat could be detected after 20h reaction while only ~1% of PS was recovered in the solution (**Figure S17**).

In order to investigate the recyclability of the Ru-Rh@MIL-101-NH_2 photosystem, the solid was recovered after 5 h reaction and assayed in an additional photocatalytic 5h run under identical conditions, through 5 successive cycles (**Figure S16**). While activity was observed at each cycle, it systematically decreased. This was obviously not due to leaching of active components as shown (**Figure S17**). This was not due either to framework collapse as the crystalline structure was maintained (**Figure S15**), thus overcoming some main drawbacks of bimetallic heterogeneous MOF photocatalysts where leaching of catalyst and photosensitizer occurs during reaction.[17] The decrease in catalytic activity is most likely related to the well-known intrinsic photodegradation/photobleaching of the Ru(bpy)$_3$ components.[27] Interestingly the overall amount of formate formed after 4 cycles of 5 h reaction is the same than that after 20 h of continuous photocatalysis (about 0.8 μmol).

Conclusion

In summary, we have reported with the Rh-Ru@MIL-101-NH_2 composite a simple method for the immobilization of a full molecular {cat, PS} photosystem within a porous MOF host for the reduction of CO_2 under visible light. First, the irreversible co-adsorption of the molecular Cp*Rh-catalyst and Ru-based photosensitizer is successfully achieved in the MOF's pores. The use of carboxylated functionalized complexes gives rise to enhanced host-guest interactions and prevents them from further leaching out including during photocatalysis. Second, we demonstrate that the confinement of both the molecular catalyst and photosensitizer within an "inert" MOF host is indeed operational, allowing the photoreduction of CO_2 to occur in similar conditions than in homogenous catalysis. Still, the MOF cavity is used here as a nanoreactor and allows to perform molecular catalysis in a heterogeneous manner thanks to the co-confinement of cat and PS into the cavity's nanospace. Third, the exclusive production of formate with the suppression of H_2 production points towards a remarkable change of selectivity of the Ru-Rh photosystem when immobilized in the Rh-Ru@MIL-101-NH_2 composite. This proof-of-principle study opens new opportunities for the design of functionalized bi-metallic and multiple-component MOFs for photocatalytic applications, while stimulating further research efforts on the optimization of {PS,cat} combinations for light-driven transformations.

Experimental Section

Experimental and computational details are reported in the Supporting Information.

Synthetic Methods

MIL-101-NH_2(Al) was synthesized according to a modified literature procedure[28]: 0.68 g (3.7 mmol) 2-amino terephthalic acid (Sigma Aldrich, 99 %) were dissolved in 100 mL of anhydrous DMF and heated to 110 °C. A solution of 1.81 g (7.4 mmol) $AlCl_3 \cdot 6H_2O$ (Sigma Aldrich, 99 %) in 50 mL anhydrous DMF was added slowly over 1h30. The resulting suspension was stirred for 3 h at 110 °C and kept at 110 °C without stirring overnight. After the mixture was cooled to room temperature, the yellow precipitate was removed by centrifugation and washed twice with 50 mL DMF. Further purification was done by Soxhlet extraction with acetonitrile over night. The yellow solid obtained was dried at 100 °C for 24 h. Yield: 0.87 g (1.2 mmol, 96 % based on molecular weight for $[Al_3O(OH)(bdc\text{-}NH_2)_3(H_2O)_2]_{24} \cdot 110H_2O$ taking mass loss from TGA into account). The desired Cp*Rh complexes were synthesized following literature [29] through the direct addition of diimine ligand to 0.5 equivalent of the commercially available $[Cp^*RhCl_2]_2$ in methanol. The reaction was complete in ca. 30 minutes at room temperature. The reaction

solution was then concentrated under vacuum. Slow addition of diethyl ether resulted in the precipitation of the desired orange product.

Impregnation experiments

Single components. In a typical experiment, each compound (PS or cat) was prepared at a chosen concentration in MeCN in a spectrophotometric cuvette and the solution is characterized by UV-visible spectroscopy. For each experiment, two samples were prepared: one for the adsorption assay and one as a control. The control cuvette contains 4 mL of PS or cat in solution in the absence of MOF. The assay cuvette contained 4 mL of the same PS/cat solution in which 5 mg of solid MOF has been added. The liquid fraction was monitored by UV-Vis spectroscopy at time intervals. Adsorption and immobilization of the soluble compound (PS or cat) into the MOF resulted in a decrease of its concentration in solution and thus a decrease of the intensity of its characteristic absorption bands. When the UV-Vis spectrum of the solution stopped changing with time, *i.e.* reaching the adsorption equilibrium, the supernatant was removed and 4 mL of fresh MECN were added into the cuvette to check whether PS/cat is released from the MOF. This was easily monitored by the reappearance and increase with time of the UV-vis spectrum of the complex of interest. This last step was repeated several times. The control experiment allowed taking into account any changes in the absorption spectra that were not related to the presence of the MOF.

Co-immobilization of [Cp*Rh(4,4'-bpydc)Cl]Cl and $[Ru(bpy)_2(4,4'\text{-bpydc})]Cl_2$. Since both $[Cp^*Rh(4,4'\text{-bpydc})Cl]^+$ and $[Ru(bpy)_2(4,4'\text{-bpydc})]^{2+}$ possess the same type of ligand, *i.e.*, carboxylic groups on bpy ligands, they may compete during the impregnation process into the MOF. In addition, Rh-complexes have a larger affinity for MIL-101-NH_2(Al) when compared to that of Ru-complexes, as found from single component impregnation experiments. To ensure the efficient electron transfer from Ru photosensitizer to Rh catalyst in CO_2 photoreduction, Ru complex in the initial solution was used in excess to the Rh complex in a 5:1 ratio.

Characterizations

The powder X-Ray diffraction measurements on the materials were collected at room temperature using a Bruker D5005 Diffractometer equipped with a Lyon-Eye detector ($Cu_{K\alpha}$ radiation, wavelengths λ = 0.154178 nm).

N_2 adsorption isotherm. The N_2 adsorption/desorption isotherms at 77 K were measured on a BELSORP-mini II. Prior to measurements the samples were degassed under vacuum (~ 10^{-4} mbar) at 100 °C for at least 12 h. BET surface area was determined for all samples in the pressure range $0.01 < p/p_0 < 0.1$.

Liquid state ^{1}H NMR spectra were recorded on a Bruker Ascend 400 spectrometer (9.4 T, ^{1}H at 400.13 MHz), 64 scans, zg30. Prior to measurement the solids were dissolved in DMSO-d6/HF solution, all spectra were referenced against the deuterated solvent.

Elemental analyses were done by ICP-OES ACTIVA (Jobin Yvon) for heavy elements (Rh, Al, Ru).

Photocatalytic assays

Photochemical reactions were performed using a 300 W, high-pressure Xe arc lamp (Oriel Instruments). The beam was passed through an infrared filter, a collimating lens, a filter holder equipped with a 415 nm band pass filter. Samples were prepared in a 1 cm path length quartz cuvette (Starna) which was placed in a temperature controlled cuvette holder (Quantum Northwest) maintained at 20°C with a circulated water bath. In all experiments, the solid MOF sample was suspended in 1 mL of a MeCN/TEOA mixture used as the solvent, saturated with CO_2 via directly bubbling CO_2 through the solution mixture for 10 minutes. As the system is not homogeneous vigorous stirring of the solution was carried out during irradiation. We used 5 mg for assays for the single component MOF and 2.5 mg for the Rh-Ru@MOF assays.

H_2 detection: H_2 measurements were performed by gas chromatography on a Shimadzu GC-2014 equipped with a Quadrex column, a Thermal Conductivity Detector and using N_2 as a carrier gas. Gas chromatography calibration curves were made by sampling known volumes of H2 gas. The typical volume of gas injected was 50 µL.

Formate detection: Formate concentration was determined using a Metrohm 883 Basic IC plus ionic exchange chromatography instrument, using a Metrosep A Supp 5 column and a conductivity detector. A typical measurement requires the sampling of 200 µL of solution, followed by a 100-fold dilution in deionised 18 MΩ water and injection of 20 µL into the instrument.

Computational Chemistry

In short, for probing the host-guest potential energy surface, we applied a simulated annealing (SA) procedure. Low energy adsorption sites for the Rh-complex were thus identified by repeatedly searching the configurational space of the {Rh-complex, MOF} system as the temperature was slowly decreased. In this conformational search, the Rh-complex was treated as a rigid body and host framework as the fixed-atom host. Only the position and orientation of the Rh-complex were sampled during the simulated annealing procedure, allowed to visit all possible void volumes of the MIL-101-NH_2. Calculations were performed fixing the loading of Rh-complex at one per large cage, thus mimicking the experimental loading obtained from UV-visible spectroscopy and elemental analysis. In the next step, a more precise geometry of the Rh-complex adsorption site into the MIL-101-NH_2 pore was further determined through density functional theory calculations performed in the Vienna Ab-initio Simulation Package VASP.[30] Considering the extremely large size of the periodic system generated above at the simulated annealing step, DFT geometry optimizations were performed on a cluster cleaved from the optimized unit-cell of the two lowest energy conformations. A planewave basis set with the projector augmented wave (PAW) scalar-relativistic pseudopotentials[31] was employed for all geometry and electronic calculations. The electron-ion interactions were described by the PAW method in the implementation of Kresse and Joubert.[32] Geometry optimizations were performed with the Perdew-Burke-Ernzerhof (PBE) exchange-correlation functional.[33] The long-range weak dispersion interactions were taken into account using the semi empirical vdW method of Grimme DFT-D3.[34] A plane-wave cutoff of 400 eV, for the construction of the electronic wave functions, was found to be suitable for convergence of the system. The integration over the irreductible Brillouin zone was carried out using the gamma point. Atomic positions were optimized until the forces on all atoms were smaller than 0.02 eV Å-1. Once the {Rh-complex, MIL-101-NH_2} cluster was fully optimized, the binding

energy between the Rh-complex and the MOF was then calculated as: $E_{binding\ energy} = E_{\{Rh\text{-}complex,MOF\}} - E_{\{Rh\text{-}complex\}} - E_{\{MOF\}}$, where $E_{\{Rh\text{-}complex\}}$ and $E_{\{MOF\}}$ are single point calculations of the Rh-complex and MOF, respectively, extracted from the fully optimized {MOF, Rh-complex} cluster. Further details on the simulated annealing procedure and DFT calculations are given in SI.

Acknowledgements

F.M.W. gratefully acknowledges financial support from the Deutsche Forschungsgemeinschaft (DFG, Postdoctoral Research Fellowship, grant number WI 4721/1-1). The authors are very grateful to N. Cristin and P. Mascunan for ICP-OES analysis. The calculations were performed by using the HPC resources from GENCI (CINES/TGCC/IDRIS) through Grant 2016-097343. X.W. acknowledges support from PSL University. This work was supported by the French State Program 'Investissements d'Avenir' (Grants "LABEX DYNAMO", ANR-11-LABX-0011).

Keywords: metal-organic frameworks • photocatalysis • CO_2 reduction • heterogeneous catalysis • nanoreactor

References

[1] (a) C. D. Wu, M. Zhao *Adv. Mater.* **2017**, 29, 1605446. (b) R. M. Bullock, A. K. Das, A. M. Appel *Chem. Eur. J.* **2017** 23, 7626-7641. (c) N. Elgrishi, M. Chambers, X. Wang, M. Fontecave *Chem. Soc. Rev.* **2017**, 46, 761-796)12.

[2] (a) J. L. Wang, C. Wang, W. Lin, *ACS Catal.* **2012**, 2, 2630−2640. (b) Y. Bai, Y. Dou, L.-H. Xie, W. Rutledge, J.-R. Li, H.-C. Zhoub, *Chem. Soc. Rev.* **2016**, 45, 2327. (b) S. Wang and X. Wang *Small* **2015**, 11, No. 26, 3097–3112.

[3] (a) D. Farrusseng, S. Aguado, C. Pinel *Angew. Chem. Int. Ed.* **2009**, 48, 7502-7513. (b) S.M. Cohen, *Chem. Rev.* **2012**, 112 , 970-1000. (c) W. Lu, Z. Wei, Z.-Y. Gu, T.-F. Liu, J. Park, J. Park, J. Tian, M. Zhang, Q. Zhang, T. Gentle III, M. Bosch, H.-C. Zhou *Chem. Soc. Rev.* **2014**, 43, 5561.

[4] (a) C. Wang, Z. Xie, K. E. deKrafft, W. Lin, *J. Am. Chem. Soc.* **2011**, 133, 13445. (b) M. A. Nasalevich, M. van der Veen, F. Kapteijn, J. Gascon, *CrystEngComm.* **2014**, 16, 4919-4926. (c) J. L. Wang, C. Wang, W. Lin, *ACS Catal.* **2012**, 2, 2630-2640. (d) Y. Horiuchi, T. Toyao, M. Takeuchi, M. Mastuoka, M. Anpo, *Phys. Chem. Chem. Phys.* **2013**, 15, 13243-13253. (e) T. Zhang, W. Lin, *Chem. Soc. Rev.* **2014**, 43, 5982-5993. (f) M. E. Foster, J. D. Azoulay, B. M. Wong, M. D. Allendorf, *Chem. Sci.* **2014**, 5, 2081-2090.

[5] (a) C.-C. Wang, J. R. Li, X.-L. Lv, Y.-Q. Zhang, G. Guo, *Energy Environ. Sci.* **2014**, 7, 2831-2867. (b) J. Long, S. Wang, Z. Ding, S. Wang, Y. Zhou, L. Huang, X. Wang, *Chem. Commun.* **2012**, 48, 11656-11658. (c) P. Wu, C. He, J. Wang, X. Peng, X. Li, Y. An, C. Duan, *J. Am. Chem. Soc.* **2012**, 134, 14991-14999.

[6] (a) K. Meyer, M. Ranocchiari, J. A. van Bokhoven, *Energy Environ. Sci.* **2015**, 8, 1923-1937. (b) L. Chi, Q. Xu, X. Liang, J. Wang, X. Su, *Small* **2016**, 12, 1351-1358.

[7] (a) C. Gomes Silva, I. Luz, F. X. Llabres i Xamena, A. Corma, H. Garcia, *Chem. Eur. J.* **2010**, 16, 11133-11138. (b) S. Pullen, H. Fei, A. Orthaber, S. Cohen, S. Ott, *J. Am. Chem. Soc.* **2013**, 45, 16997-17003. (c) K. Sasan, Q. Lin, C. Mao, P. Feng, *Chem. Commun.* **2014**, 50, 10390-10393. (d) M. A. Nasalevich, R. Becker, E. V. Ramos-Fernandez, S. Castellanos, S. L. Veber, M. V. Fedin, F. Kapteijn, J. N. H. Reek, J. I. van der Vlugt, J. Gascon *Energy Environ. Sci.* **2015**, 8, 364-375.

[8] (a) R. N. Amador, M. Carboni, D. Meyer *Materials Letters* **2016**, 166, 327–338. (b) J. W. Maina, C. Pozo-Gonzalo, L. Kong, J. Schütz, M. Hill, L. F. Dumée *Mater. Horiz.* **2017**, 4, 345-361. (c) C.-C. Wanga, Yan-Qiu Zhang, J. Li, P. Wang *J. Mol. Struct.* **2015**, 1083, 127–136. (d) Y. Chen, D. Wang, X. Deng, Z. Li. Catal. *Sci. Technol.* **2017**, 7, 4893. (e) S. Wang, W. Yao,; J. Lin, Z. Ding, X. Wang *Angew. Chem. Int. Ed.*, **2014**, 53, 1034-1038.

[9] (a) M. B. Chambers, X. Wang, L. Ellezam, O. Ersen, M. Fontecave, C. Sanchez, L. Rozes, C. Mellot-Draznieks, *J. Am. Chem. Soc.* **2017**, 139, 8222-8228. (b) Y. Fu, D. Sun, Y. Chen, R. Huang, Z. Ding, X. Fu, Z. Li *Angew. Chem. Int. Ed.* **2012**, 51, 3364-3367. (c) D. Sun, Y. Fu, W. Liu, L. Ye, D. Wang, L. Yang, X. Fu, Z. Li, *Chem. Eur. J.* **2013**, 19, 14279-14285. (d) Y. Lee, S. Kim, J. K. Kang, S. M. Cohen, *Chem. Commun.* **2015**, 51, 5735-5738. (e) D. Sun, W. Liu, M. Qiu, Y. Zhang, Z. Li, *Chem. Commun.* **2015**, 51, 2056–2059. (f) D. Wang, R. Huang, W.Liu, D. Sun, Z. Li *ACS Catal.* **2014**, 4, 4254-4260. (g) H.-Q. Xu, J. Hu, D. Wang, Z. Li, Q. Zhang, Y. Luo, S.-H. Yu, H.-L. Jiang *J. Am. Chem. Soc.* **2015**, 137, 13440-13443. (h) D. S. Chen, H. Z. Xing, C. G. Wang, Z. M. Su, *J. Mater. Chem. A* **2016**, 4, 2657-2662.

[10] (a) C. H. Hendon, D. Tiana, M. Fontecave, C. Sanchez, L. D'Arras, C. Sassoye, L. Rozes, C. Mellot-Draznieks, A. Walsh, *J. Am. Chem. Soc.* **2013**, 135, 30, 10942. (b) S. Hamad, N. C. Hernandez, A. Aziz, A. R. Ruiz-Salvador, S. Calero, R. Grau-Crespo. *J. Mater.Chem.* **2015**, 3, 23458-23465.

[11] J. H. Cavka, S. Jakobsen, U. Olsbye, N. Guillou, C. Lamberti, S. Bordiga, K. P. Lillerud, *J. Am. Chem. Soc.* 2008, 130, 13850-13851.

[12] (a) I. Senkovska, F. Hoffmann, M. Fröba, J. Getzschmann, W. Böhlmann, S. Kaskel, *Microporous Mesoporous Mater.* **2009**, 122, 93-98. (b) E. D. Bloch, D. Britt, C. Lee, C. J. Doonan, F. J. Uribe-Romo, H. Furukawa, J. R. Long, O. M. Yaghi, *J. Am. Chem. Soc.* **2010**, 132, 14382-14384.

[13] (a) R. Y. Huang, Y. Peng, C. Wang, Z. Shi, W. B. Lin, *Eur. J. Inorg. Chem.* **2016**, 27, 4358–4362. (b) U. J. Ryu, S. J. Kim, H. K. Lim, H. J. Kim, K. M. Choi, J. K. Kang, *Sci. Rep.* **2017**, 7, 612. (c) K. M. Choi, D. Kim, B. Rungtaweevoranit, C. A. Trickett, J. T. D. Barmanbek, A. S. Alshammari, P. D. Yang, O. M. Yaghi, *J. Am. Chem. Soc.* **2017**, 139, 356–362.

[14] (a) S. Zhang, L. Li, S. Zhao, Z. Sun, J. Luo *Inorg. Chem.* **2015**, 54, 8375-8379. (b) S. Zhang, L. Li, S. Zhao, Z. Sun, M. Hong, J. Luo, *J. Mater. Chem. A* **2015**, 3, 15764-15768. (c) D. Sun, Y. Gao, J. Fu, X. Zeng, Z. Chen, Z. Li, *Chem. Comm.* **2015**, 51, 2645-2648. (d) T. Kajiwara, M. Fujii, M. Tsujimoto, K. Kobayashi, M. Higuchi, K. Tanaka, S. Kitagawa, *Angew. Chem.* **2016**, 128, 2697-2700.

[15] M. B. Chambers, X. Wang, N. Elgrishi, C.H. Hendon, A. Walsh, J. Bonnefoy, J. Canivet, E. A. Quadrelli, D. Farrusseng, C. Mellot-Draznieks, M. Fontecave *ChemSusChem.* **2015**, 8, 603-608.

[16] H. Fei, M. D. Sampson, Y. Lee, C. P. Kubiak, S. M. Cohen, *Inorg. Chem.* **2015**, 54, 6821–6828.

[17] (a) C.-C. Hou, T.-T. Li, S. Cao, Y. Chen, W.F. Fu, *J. Mater. Chem. A*, **2015**, 3, 10386. (b) D. Sun, Y. Gao, J. Fu, X. Zeng, Z. Chen, Z. Li *Chem. Comm.* **2015**, 2645-2648.

[18] J. Juan-Alcañiz, J. Gascon, F. Kapteijn, *J. Mat. Chem.* **2012**, 22, 10102-10118.

[19] (a) J. Han, D. Wang, Y. Du, S. Xi , Z. Chen, S. Yin, T. Zhou, R. Xu, *Appl. Cat. A* **2016**, 521, 83-89. (b) M. A. Nasalevich, R. Becker, E. V. Ramos-Fernandez, S. Castellanos, S. L.Veber, M. V. Fedin, F. Kapteijn, J. N. H. Reek, J. I. van der Vlugt, J. Gascon, *Energy Environ. Sci.* **2015**, 8, 364-375. (c) Z. Li, J.-D. Xiao, H.-L. Jiang *ACS Catal.* **2016**, 6, 5359-5365. (d) X. J. Kong, Z. K. Lin, Z. M. Zhang, T. Zhang, W. B. Lin. *Angew. Chem. Int. Ed.* **2016**, 55, 6411-6416. (b) Z. M. Zhang, T. Zhang, C. Wang, Z. Lin, L. S. Long, W. Lin, *J. Am. Chem. Soc.* **2015**, 137, 3197-3200.

[20] G. Paille, M. Gomez-Mingot, C. Roch-Marchal, B. Lassalle-Kaiser, P. Mialane, M. Fontecave, C. Mellot-Draznieks, A. Dolbecq. *J. Am. Chem. Soc.* **2018**,140, 3613-3618.

[21] (a) G. Férey, C. Mellot-Draznieks, C. Serre, F. Millange, J. Dutour, S. Surblé, I. Margiolaki, *Science* **2005**, 309, 2040-2042. (b) M. Latroche, S. Surblé, C. Serre, C. Mellot-Draznieks, P. L. Llewellyn, J.-H. Lee, J.-S. Chang, S. H. Jhung, G. Férey, *Angew. Chem., Int. Ed.* **2006**, 45, 8227-8231. (c) M. Hartmann, M. Fischer *Microporous Mesoporous Mater.* **2012**, 164, 38-43.

(d) P. Serra-Crespo, E. V. Ramos-Fernandez, J. Gascon, F. Kapteijn *Chem. Mater.* **2011**, 23, 2565-2572.
[22] P. Serra-Crespo, E. V. Ramos-Fernandez, J. Gascon, F. Kapteijn, *Chem. Mater.* **2011**, 23, 2565-2572.
[23] (a) A. K. Mengele, S. Rau, *Inorganics* **2017**, 5, 35. (b) J. Canivet, G. Süss-Fink, P. Stepnicka, *Eur. J. Inorg. Chem.* **2007**, 4736-4742. (c) E. Steckhan, S. Hermann, R. Ruppert, E. Dietz, M. Frede, E. Spika, *Organometallics* **1991**, 10, 1568-1577.
[24] C. Caix, S. Chardon-Noblat, A. Deronzier, *J. Electroanal. Chem.* **1997**, 434,163-170.
[25] F. M. Wisser, P. Berruyer, L. Cardenas, Y. Mohr, E. A. Quadrelli, A. Lesage, D. Farrusseng, J. Canivet, *ACS Catal.* **2018**, 8, 1653-1661.
[26] C. Hansch, A. Leo, R.W. Taft, *Chem. Rev.* **1991**, 91 ,165-195.
[27] Hawecker, J.; Lehn, J.-M. *J. Chem. Soc., Chem. Comm.* **1985**, 2, 56-58.
[28] Hartmann, M.; Fischer, M. Microporous Mesoporous Mater. **2012**, 164, 38.
[29] Brewster, T. P.; Miller, A. J. M.; Heinekey, D. M.; Goldberg, K. I. *J. Am. Chem. Soc*. **2013**, 135 (43), 16022–16025.
[30] (a) G. Kresse, J. Furthmüller, *Phys. Rev. B* **1996**, 54, 11169-11186. (b) G. Kresse, J. Furthmüller, *Comput. Mater. Sci.* **1996**, 6, 15-50.
[31] P. E. Blöchl, *Phys. Rev. B* **1994**, 50, 17953-17979
[32] G. Kresse, D. Joubert, *Phys. Rev. B.* **1999**, 59, 1758-1775.
[33]J. P. Perdew, K. Burke, M. Ernzerhof, *Phys. Rev. Lett.* **1996**, 77, 3865-3868.
[34] S. Grimme, J. Antony, S. Ehrlich, H. Krieg, *J. Chem. Phys.* **2010**, 132, 154104.